Rare earth focused ion beam implantation utilizing Er and Pr liquid alloy ion sources

L. C. Chao, B. K. Lee, C. J. Chi, J. Cheng, I. Chyr, and A. J. Steckl[a)]
Nanoelectronics Laboratory, University of Cincinnati, Cincinnati, Ohio 45221-0030

(Received 1 June 1999; accepted 16 August 1999)

We have developed procedures for the fabrication of Er–Ni and Pr–Pt liquid alloy ion sources (LAIS). Er^{2+}beam with target current of ~100 pA and Pr^{2+} beams with target current of ~200 pA were obtained, which correspond to 50% and 80% of the total target current, respectively. Both Er–Ni and Pr–Pt alloys oxidize quickly once exposed to air. Er–Ni source lifetimes were generally larger than 200 μA h. The source lifetimes of Pr–Pt LAISs were approximately 30 μA h, limited by oxide contamination and wettability problems. Visible photoluminescence has been observed from Er- or Pr-doped GaN, Al_2O_3, and ZBLAN glass using focused ion beam direct write implantation.
 [S0734-211X(99)08306-7]

I. INTRODUCTION

Rare earth ions have been widely doped into insulators such as fluoride and oxide compounds for laser and optical communication applications.[1] Among the rare earths, erbium and praseodymium have drawn the most interest because of the Er^{3+} emission at 1.54 μm and Pr^{3+} emission at 1.3 μm, which correspond to wavelengths for minima in absorption and dispersion of silica optical fibers. If sufficient light emission can be obtained from rare-earth-doped semiconductors, monolithic optoelectronic devices will be realized and this will greatly simplify and reduce the cost of modern optical communication systems. A major research effort has been devoted to the incorporation of Er in Si.[2,3] However, progress in Er-doped Si has been limited due to the low equilibrium solubility of Er in Si ($\sim 10^{18}$ atoms/cm^3) and the thermal quenching effect.[4]

The thermal quenching effect could be reduced in wide band gap semiconductor (WBGS) materials.[5] Recently visible and/or infrared emission has been obtained from a variety of erbium doped WBGS materials, such as SiC,[6] GaAs,[7] InP,[8] and GaN.[9] Among them, GaN has drawn the most attention. In addition to the commonly observed infrared emission, visible photoluminescence (PL), electroluminescence (EL), or cathodoluminescence (CL) have been obtained from Pr,[10,11] Eu,[12] Dy,[13] Er,[13–15] and Tm[16] doped GaN. Rare earth elements were added during growth or by ion implantation. Waveguides, lasers, and light-emitting diodes (LEDs) have been fabricated using traditional lithography techniques. An alternative method of fabricating the optoelectronic devices and future optoelectronic integrated circuits (OEIC) is using focused ion beam (FIB) implantation and/or micromilling. FIB technology is now well established and has found widespread application in the semiconductor industry, where FIBs are used for failure analysis, transmission electron microscopy specimen preparation, circuit, and mask modification. FIB micro and nanofabrication can be utilized to reduce the complexity required in conventional OEIC fabrication technology (in particular, lithography, etching, and implantation), which has to satisfy various requirements for different components fabricated on the same substrate.[17]

The success of FIB technology is due to the invention of liquid metal ion sources (LMIS).[18] A LMIS can be made in needle or capillary form. The liquid metal is drawn into a Taylor cone where ion emission is formed.[19] A modern FIB system with a LMIS can produce a focused beam with a target current of 50–100 pA and a scanning resolution of 20–50 nm.[18] Almost any metallic element can be made into the form of LMIS or liquid alloy ion sources (LAIS). In the latter case, binary or even ternary alloy may be used. The liquid metal or liquid alloy should have low vapor pressure and good wettability with the substrate.[20] Er has a high melting point (1529 °C) and a high vapor pressure at its melting point (≈1 Torr). Pr also has a high melting point (931 °C), but with a lower vapor pressure at its melting point ($\approx 5 \times 10^{-7}$ Torr).[21] These properties make them unsuitable for elemental LMIS. Instead, they must be made in the form of an alloy source by combining with another material in order to lower the melting point and, hopefully, the vapor pressure. The melting points of attractive binary alloy candidates with the atomic percentage ratios shown in the parenthesis are Er(69):Ni(31) at 765 °C, Pr(87):Pt(13) at 718 °C, and Pr(78):Ag(22) at 586 °C.[22]

II. LAIS FABRICATION

The alloys are made by mixing erbium (3N), nickel (3N), praseodymium (3N), platinum (3N), and silver (3N) powders at the appropriate ratios. The mixed powder is then put in a molybdenum crucible in a separate vacuum system. The ion source is made by using a 250 μm diameter tungsten wire. The wire is twisted around a 0.125 in. outer diameter Al_2O_3 tube in order to be fitted into the ion gun module of a NanoFab 150 FIB system. The tip is mechanically polished and then electrochemically etched in a NaOH solution until the end radius is approximately 10 μm. After the alloy reaches its molten state, the tip is dipped into the crucible for two minutes. The source is then tested *in situ* by applying appro-

a)Electronic mail: a.steckl@uc.edu

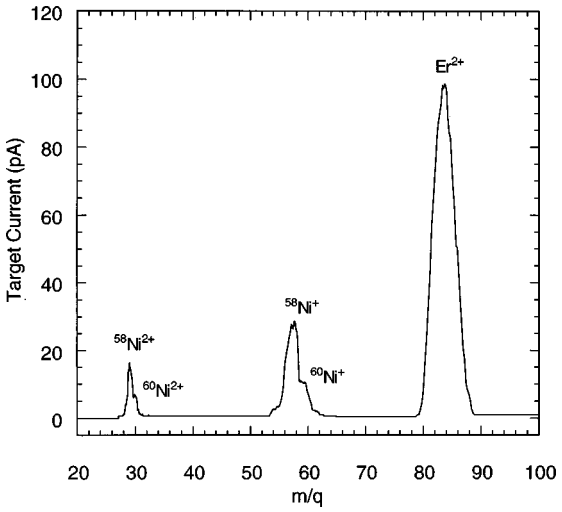

FIG. 1. Mass spectrum of the target current of an Er–Ni LAIS. The alloy is formed by mixing Er and Ni powders at an atomic percent ratio of 69:31. The eutectic alloy has a melting point of 765 °C. The total target current is 190 pA. The source heater current is 6.5 A.

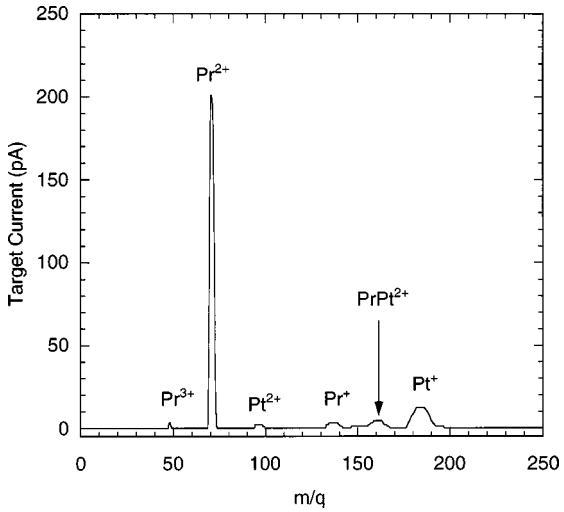

FIG. 2. Mass spectrum of the target current of a Pr–Pt LAIS. The alloy is formed by mixing Pr and Pt powders at an atomic percent ratio of 87:13. The eutectic alloy has a melting point of 718 °C. The total target current is 250 pA. The source heater current is 5.5 A.

priate voltage and heating current to the source. A detailed description of the fabrication process can be found in Ref. 23.

III. RESULTS

Figure 1 shows the mass spectrum of the target current from an Er–Ni LAIS. The total ion emission current is 15 μA and the source heating current is 6.5 A. Figure 1 indicates that doubly charged erbium ions (Er^{2+}) represent the single largest component of the beam (95 pA), producing approximately 50% of the total target current which was 190 pA. The source oxidizes quickly once exposed to air. This must be minimized to maintain source lifetime and stability. The average lifetime of Er–Ni LAIS is generally larger than 200 μA h. In Fig. 1, one can also find that the ion beam components associated with the two main nickel isotopes Ni^{58} and Ni^{60} can be distinguished. Their respective ion currents are present in the same ratio as their natural abundance ($\sim$2.5).[23]

The mass spectrum of the target current of a Pr–Pt LAIS is shown in Fig. 2. The total ion emission current is 15 μA and the source heating current is 5.5 A. Pr^{2+}represents the single largest component of the beam (200 pA), producing approximately 80% of the total target current which is 250 pA. The average Pr–Pt LAIS lifetime when tested *in situ* was larger than 60 μA h. After the Pr–Pt sources were transferred to the FIB system, the lifetime averaged only $\sim$30 μA h. Figure 3 shows a scanning electron microscopy (SEM) micrograph of the shank of a Pr–Pt LAIS after its emission quenches. One can notice the discontinuity of the alloy between the reservoir and the tip, which leads to a reduced source lifetime. Elemental Pr LMISs were also fabricated, but we were not able to extract an ion current. This may be due to the source heating capability of our current system which is limited to 10 A. Another attractive Pr alloy source candidate is Pr–Ag which has a much lower melting point of 586 °C. Figure 4 shows the mass spectrum of a Pr–Ag LAIS. The total emission current is 15 μA and the source heater current is 4.5 A. For this alloy, Pr^{2+} still represents the single largest component of the beam (140 pA), producing approximately 70% of the total target current which is 200 pA. The source lifetimes of Pr–Ag LAISs were generally less than 10 μA h. Extreme care must be practiced to keep the temperature of the Pr–Ag alloy just above its melting point but still below its boiling point. This leads to a high vapor pressure problem which hinders its practical use. The Pr–Ag LAIS has a similar alloy discontinuity problem. Both Pr–Pt and Pr–Ag alloy oxidize quickly once exposed to air.

IV. FIB IMPLANTATION OF Pr AND Er

The implantation was performed in the same FIB system. Pr^{2+} and Er^{2+} beams were accelerated to high energy and implantation was carried out at room temperature on GaN, Al_2O_3, or ZBLAN. The ZBLAN glass sample has a

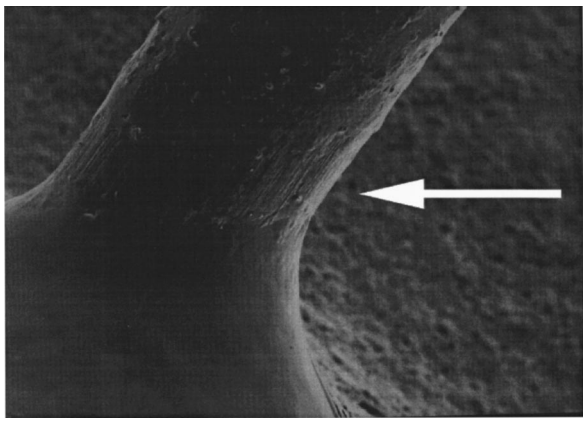

FIG. 3. SEM micrograph of the shank of a Pr–Pt LAIS after ion emission quenches. The arrow points to the discontinuity of the alloy between reservoir and tip.

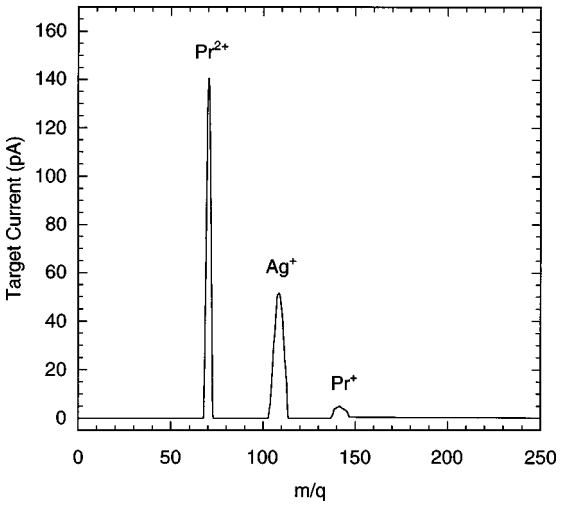

FIG. 4. Mass spectrum of the target current of a Pr–Ag LAIS. The alloy is formed by mixing Pr and Ag powders at an atomic percent ratio of 78:22. The eutectic alloy has a melting point of 586 °C. The total target current is 200 pA. The source heater current is 4.5 A.

composition (mol %) of $ZrF_4(53)-BaF_2(20)-LaF_3(4)-NaF(20)-AlF_3(3)$. Figure 5 shows a Pr-implanted GaN film grown on sapphire by molecular beam epitaxy (MBE).[11] The implanted pattern is a 141 μm×141 μm square. The implantation energy and dose were 290 keV and 4.7×10^{14} atoms/cm^2, respectively. After FIB implantation, the sample was annealed at 1050 °C in Ar for 1 h. Figure 5 shows that when the implanted pattern is under ultraviolet excitation (He–Cd laser at 325 nm), it ''glows'' with a red color. The main photoemission occurs at a wavelength of 650 nm, with a very narrow FWHM ~1.2 nm. This emission is due to the $^3P_0\rightarrow{}^3F_2$ inner shell transition of Pr^{3+} ions in the GaN film.[11]

Er implantation was performed on GaN, Al_2O_3, and ZBLAN. After FIB implantation, only the GaN samples were annealed at 1100 °C for 1 h in oxygen. Under simultaneous red (840 nm) and infrared (1.0 μm) laser excitation, strong green upconversion was observed at 523 and 546

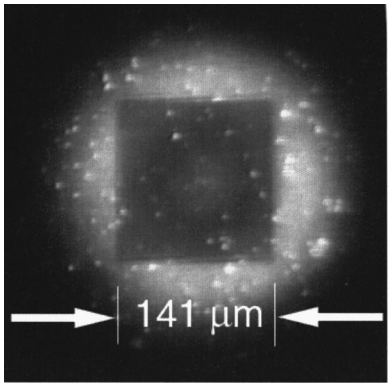

FIG. 5. Red photoluminescence from a Pr FIB-implanted GaN film grown on sapphire by MBE. The implanted pattern is a 141 μm×141 μm square. The implantation energy and dose are 290 keV and 4.7×10^{14} atoms/cm^2, respectively. The picture was obtained by exciting the FIB-implanted pattern with a He–Cd laser at 325 nm (Ref. 11).

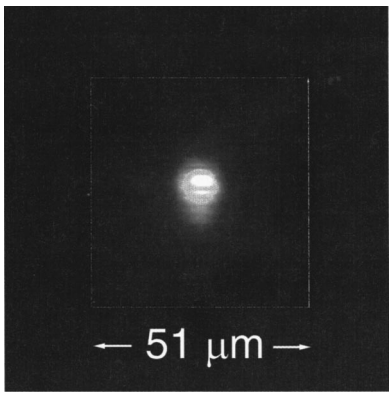

FIG. 6. Green upconversion luminescence from an Er FIB-implanted GaN film grown by MBE on sapphire. The implanted pattern is a 51 μm×51 μm square. The implantation energy and dose were 200 keV and 1.4×10^{15} atoms/cm^2, respectively. The sample was pumped with lasers at 840 nm and 1.0 μm. After FIB implantation, the sample was annealed at 1100 °C for 1 h in oxygen (Ref. 24).

nm.[24] Figure 6 shows the green upconversion from a GaN:Er sample. The implanted pattern is a 51 μm×51 μm square. The implantation energy and dose were 200 keV and 1.4×10^{15} atoms/cm^2, respectively. Figure 7 compares the green upconversion intensity from the GaN samples to that from the ZBLAN and sapphire. The two main peaks at 525–528 and 545—550 nm are due to electron transitions from the $^2H_{11/2}$ and $^2S_{3/2}$ $4f$ levels of the Er^{3+} ions in the samples. ZBLAN shows the strongest upconversion intensity, which is 40 times higher than that from GaN. The green emission from sapphire is the weakest, but it can be improved by postimplantation annealing.[25] The relative intensity between the $^2H_{11/2}$ and the $^4S_{3/2}$ emission is not the same in all three samples. A possible explanation is related to phonon energy in the three materials: ZBLAN ~72 meV,[26] GaN ~91

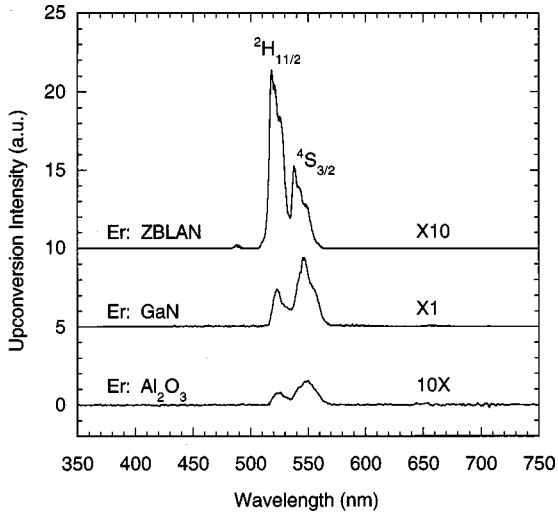

FIG. 7. Upconversion spectra of Er FIB-implanted ZBLAN (Er dose = 5.4×10^{14} atoms/cm^2, as implanted), GaN (Er dose=1.4×10^{15} atoms/cm^2, 1100 °C, 1 h, oxygen), and Al_2O_3 (Er dose=2.2×10^{15} atoms/cm^2, as implanted). The implantation is performed using a 200 keV Er^{2+} beam on all three samples.

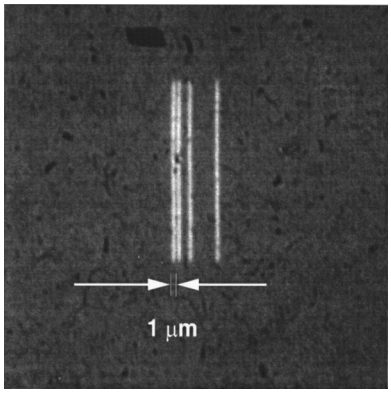

FIG. 8. 1-μm-wide Er lines on GaN patterned by FIB direct write. The implantation energy and dose are 200 keV and 1.5×10^{15} atoms/cm^2, respectively. The picture is taken under an optical microscope with no excitation lasers. The Er lines are brighter than background due to the change of index of refraction caused by FIB implantation.

meV,[27] and Al_2O_3 ~108 meV.[28] The difference between the two $4f$ levels is ~87 meV. In a material with high phonon energy, electrons are more likely to decay nonradiatively with the assistance of phonons from $^2H_{11/2}$ to $^4S_{3/2}$. This makes the $^4S_{3/2}$ level in GaN and Al_2O_3 highly populated and thus gives a higher intensity at 550 nm.

Interesting applications of Er upconversion include displays and optical memory.[29] Figure 8 shows Er lines patterned by FIB direct write on GaN. The lines are 1 μm wide by 30 μm long. The implantation energy and dose were 200 keV and 1.5×10^{15} atoms/cm^2, respectively. The picture was taken under an optical microscope before any postimplantation annealing. The Er lines are brighter than the background due to change of index of refraction caused by the FIB implantation. Currently the linewidth is limited by source drift, which can be reduced by improving the Er–Ni source stability. Ultimately, the minimum linewidth obtained will be limited by the spread of erbium isotopes.

V. SUMMARY

We have fabricated rare earth Er–Ni and Pr–Pt LAISs. Er^{2+} and Pr^{2+} beams with target current of 100 and 200 pA, respectively, were obtained. FIB implantation of Pr and/or Er were performed on GaN, Al_2O_3, and ZBLAN. Room temperature photoluminescence and upconversion were obtained. 1-μm-wide Er lines have been demonstrated on GaN films by FIB direct write.

ACKNOWLEDGMENTS

This work was supported by MRL-DOD, BMDO/ARO, and NSF contracts.

[1]A. A. Kaminkii, *Laser Crystals* (Springer, New York, 1981).
[2]H. Ennen, J. Schneider, G. Pomrenke, and A. Axmann, Appl. Phys. Lett. **43**, 943 (1983).
[3]S. Lanzerstorfer, L. Palmetshofer, and W. Jantsch, Appl. Phys. Lett. **72**, 809 (1998).
[4]T. Asatsuma, P. Dodd, J. F. Donegan, J. G. Lunney, and J. Hegarty, Mater. Res. Soc. Symp. Proc. **301**, 67 (1993).
[5]P. N. Favennec, H. L'Haridon, M. Salvi, D. Moutonnet, and Y. LeGuillou, Electron. Lett. **25**, 718 (1989).
[6]W. J. Choyke, R. P. Devaty, L. L. Clemen, M. Yoganathan, G. Pensl, and Ch. Hässler, Appl. Phys. Lett. **65**, 1668 (1994).
[7]G. S. Pomrenke, H. Ennen, and W. Haydl, J. Appl. Phys. **59**, 601 (1986).
[8]B. Lambert, A. LeCorre, Y. Toudic, C. Lhomer, G. Grandpierre, and M. Gauneau, J. Phys.: Condens. Matter **2**, 479 (1990).
[9]R. G. Wilson, R. N. Schwartz, C. R. Abernathy, S. J. Pearton, N. Newman, M. Rubin, T. Fu, and J. M. Zavada, Appl. Phys. Lett. **65**, 992 (1994).
[10]M. Garter, J. Scofield, R. Birkhahn, and A. J. Steckl, Appl. Phys. Lett. **74**, 182 (1999).
[11]L. C. Chao and A. J. Steckl, Appl. Phys. Lett. **74**, 2364 (1999).
[12]J. Heikenfeld, M. Garter, D. S. Lee, R. Brikhahn, and A. J. Steckl, Appl. Phys. Lett. **75**, 1189 (1999).
[13]H. J. Lozykowski, W. M. Jadwisienczak, and I. Brown, Appl. Phys. Lett. **74**, 1129 (1999).
[14]A. J. Steckl and R. Birkhahn, Appl. Phys. Lett. **73**, 1700 (1998).
[15]A. J. Steckl, M. Garter, R. Birkhahn, and J. Scofield, Appl. Phys. Lett. **73**, 2450 (1998).
[16]A. J. Steckl, M. Garter, D. S. Lee, J. Heikenfeld, and R. Birkhahn, Appl. Phys. Lett. **75**, 2184 (1999).
[17]A. J. Steckl, Proceedings of Advanced Workshop on Frontiers in Electronics, Tenerife, Spain, IEEE Cat. No. 97th 8292 (January 1997), p. 47.
[18]J. Orloff, Rev. Sci. Instrum. **64**, 1105 (1993).
[19]D. R. Kingham and L. W. Swanson, Appl. Phys. A: Solids Surf. **34**, 123 (1984).
[20]J. Melngailis, J. Vac. Sci. Technol. B **5**, 469 (1987).
[21]*CRC Handbook of Chemistry and Physics*, 78th ed. (Chemical Rubber, Boca Raton, FL, 1998).
[22]*Binary Alloy Phase Diagrams*, edited by T. B. Massalski (ASM International, Metals Park, OH).
[23]L. C. Chao and A. J. Steckl, J. Vac. Sci. Technol. B **17**, 1051 (1999).
[24]L. C. Chao, B. K. Lee, C. J. Chi, J. Cheng, I. Chyr, and A. J. Steckl, Appl. Phys. Lett. **75**, 1833 (1999).
[25]A. Polman, J. Appl. Phys. **82**, 1 (1997).
[26]M. J. Dejneka, MRS Bull. **23**(11), 57 (1998).
[27]M. S. Shur, Short Course at MRS 1998 Fall Meeting, Symposium G, 1998 (unpublished).
[28]H. Schober, D. Strauch, and B. Dorner, Z. Phys. B: Condens. Matter **92**, 273 (1993).
[29]E. Downing, L. Hesselink, J. Ralston, and R. Macfarlane, Science **273**, 1185 (1996).